# Supplementary Material for FRE: A Fast Method For Anomaly Detection And Segmentation

Ibrahima J. Ndiour
ibrahima.j.ndiour@intel.com
Nilesh Ahuja
nilesh.ahuja@intel.com
Utku Genc
utku.genc@intel.com
Omesh Tickoo
omesh.tickoo@intel.com

Intel Labs
Intel Corporation
USA

We present here the supplementary material for the 2023 BMVC paper *FRE: A Fast Method For Anomaly Detection And Segmentation*. While in the main text, we sometimes offered class-average results for brevity and readability, we provide here the corresponding detailed class-itemized results. In addition, we also provide a few more results showing performance across various backbones and layers, as well as pictures showing performance for a few sampled input images.

**Compute Performance:** Table 1 shows the performance of our method and compares it against the state of the art on various computing platforms (laptop-class CPU, server-class CPU and a high-end discrete GPU).

**Choice of Layers:** Tables 2, 3, 4, and 5 respectively provide a class-average summary of anomaly detection and segmentation performance for FRE across various layers of EfficientNet_B5, Resnet18, Resnet50 and VGG16 backbones. In tables 8 and 9, we show the class-itemized segmentation performance of FRE across multiple layers of a Resnet50 backbone. We observe that the middle layers generally tend to provide better detection and location performance relative to layers closer to either the input or the output.

**Additional Outputs:** Figure 1 shows a few examples of segmentation maps obtained at various layers of a Resnet50 backbone, as well as the segmentation maps obtained with the combination of 3 layers. Figure 2 shows examples of the segmentation maps produced by FRE with a single layer, and with the combination.

**Implementation strategies:** Figure 3 shows the (class-itemized) empirical validation of the different implementation strategies presented in the main paper.It is seen that all strategies

converge to the same anomaly detection performance thereby demonstrating that the three strategies are basically equivalent.

**Sensitivity to parametrization:** Figures 4 and 5 provide the class-itemized detection and segmentation performance for FRE while varying the only parameter of the method, for multiple layers of a Resnet50 backbone. These figures not only show insensitivity to parametrization, but they also give a more detailed view of the performance of the method.

**Choice of backbones:** Tables 6 and 7 shows detailed class-itemized pixel-wise AUROC metrics for the segmentation benchmark and for FRE across backbones.

| | Training Time (↓) | | | | Inference frames-per-sec (↑) | | |
|---|---|---|---|---|---|---|---|
| | PatchCore[8] | AST[8] | FRE-AEt | FRE-PCA | PatchCore[8] | AST[8] | FRE |
| NVidia 2080-Ti | 24s | 7min 22s | 5.9s | **2.8s** | 18.4 | 19.6 | **313.1** |
| Intel Xeon 8280 | 3mn 38s | 25min 24s | 1min 18s | **6.3s** | 7.11 | 11.8 | **52.6** |
| Intel i7-1270P | 4mns 5s | 5hr 8min | 2min 52s | **22.8s** | 1.28 | 2.8 | **16.4** |

Table 1: Training times and inference framerates evaluated on different computing platforms.

| | features.1 | features.2 | features.3 | features.4 | features.5 | features.6 |
|---|---|---|---|---|---|---|
| Avg AUROC | 74.7 | 86.6 | 89.5 | 95.0 | 97.6 | 98.6 |
| Avg PRO | 71.7 | 88.7 | 85.6 | 83.8 | 82.7 | 59.8 |
| Avg pixel-wise AUROC | 88.4 | 96.4 | 95.8 | 94.5 | 94.5 | 85.9 |

Table 2: FRE EfficientNet_B5 Performance across layers

| | Layer1 | Layer2 | Layer3 | Layer4 |
|---|---|---|---|---|
| Avg AUROC | 88.3 | 93.5 | 95.4 | 91.4 |
| Avg PRO | 85.3 | 90.5 | 90.2 | 68 |
| Avg pixel-wise AUROC | 94.3 | 96.8 | 97.3 | 92 |

Table 3: FRE Resnet18 Performance across layers

| | Layer1 | Layer2 | Layer3 | Layer4 |
|---|---|---|---|---|
| Avg AUROC | 87.9 | 90.7 | 96.0 | 91.9 |
| Avg PRO | 85.5 | 92.5 | 91.3 | 71.3 |
| Avg pixel-wise AUROC | 94.7 | 97.8 | 97.4 | 93.2 |

Table 4: FRE Resnet50 Performance across layers

| | feat.8 | feat.11 | feat.13 | feat.15 | feat.18 | feat.20 | feat.22 | feat.25 | avgpool |
|---|---|---|---|---|---|---|---|---|---|
| Avg AUROC | 84.0 | 88.8 | 89.5 | 90.2 | 90.1 | 90.8 | 92.2 | 93.0 | 91.6 |
| Avg PRO | 83.4 | 90.2 | 90.9 | 89.4 | 89.1 | 88.7 | 87.1 | 83.2 | NA |
| Avg Pixel-wise AUROC | 93.9 | 97.3 | 97.4 | 96.7 | 96.7 | 96.3 | 95.7 | 95.6 | NA |

Table 5: FRE VGG16 Performance across layers

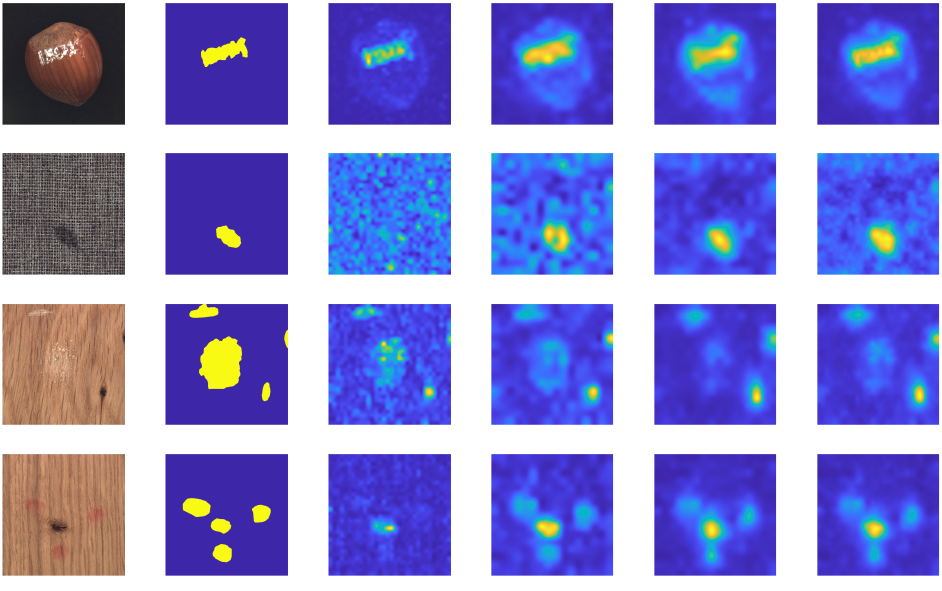

Figure 1: Using a Resnet50 backbone, for each row: input image, ground truth segmentation mask, FRE segmentation map obtained with layer1, FRE segmentation map obtained with layer2, FRE segmentation map obtained with layer3, FRE segmentation map obtained with the combination of the 3 layers (layer1, layer2 and layer3).

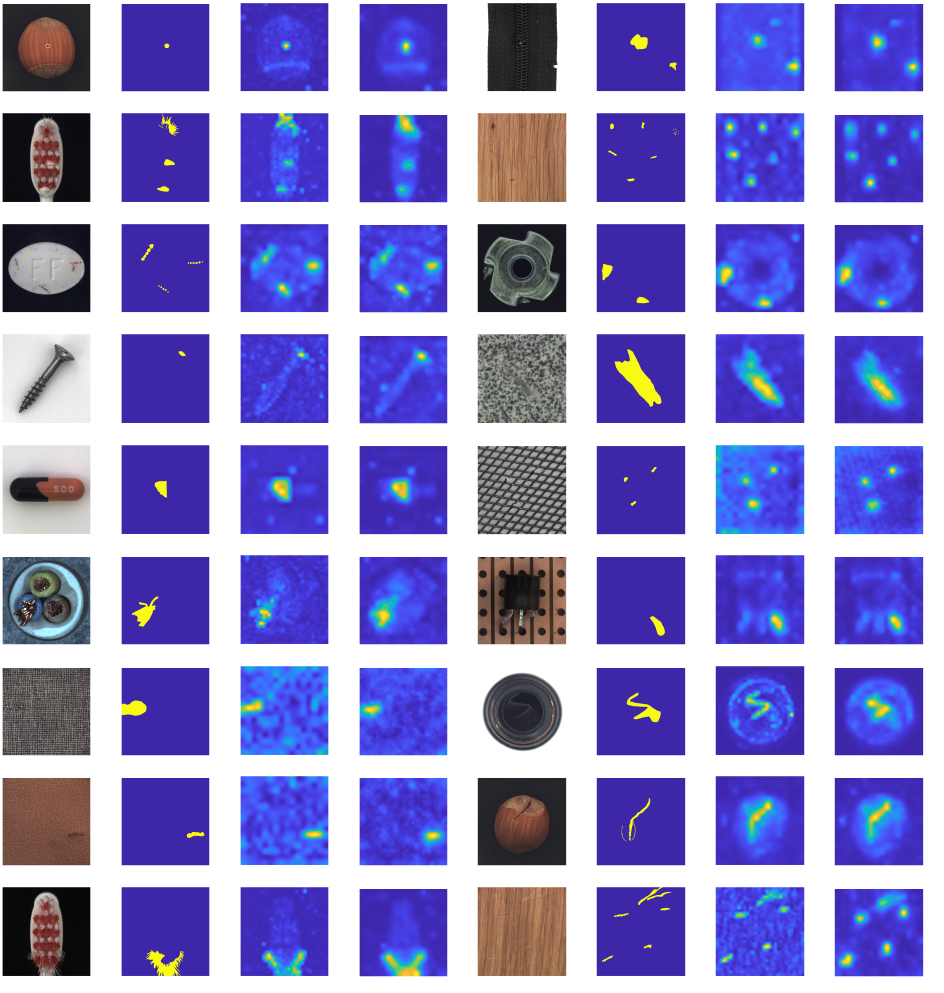

Figure 2: From left to right, each set of four images comprises: Original image, ground truth segmentation mask, anomaly heatmap using FRE (our method) from a single layer, anomaly heatmap using FRE from three layers.

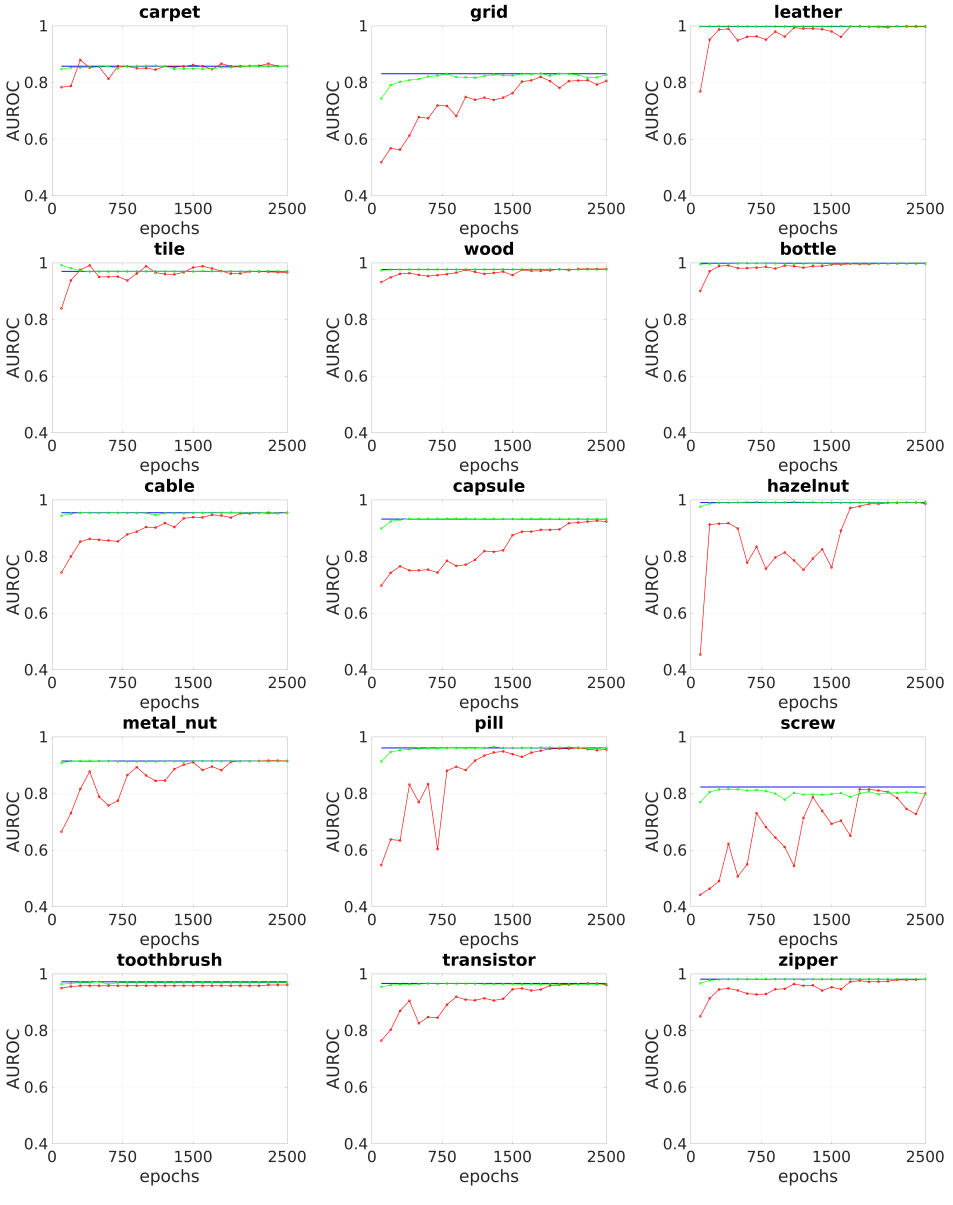


Figure 3: Class-itemized AUROC detection results for FRE-PCA (blue), FRE-AE (red) and FRE-AEt (green) with Resnet50 layer3. For FRE-AE and FRE-AEt, snapshots of the models being learned after every 100 epochs are used to show the convergence to FRE-PCA.

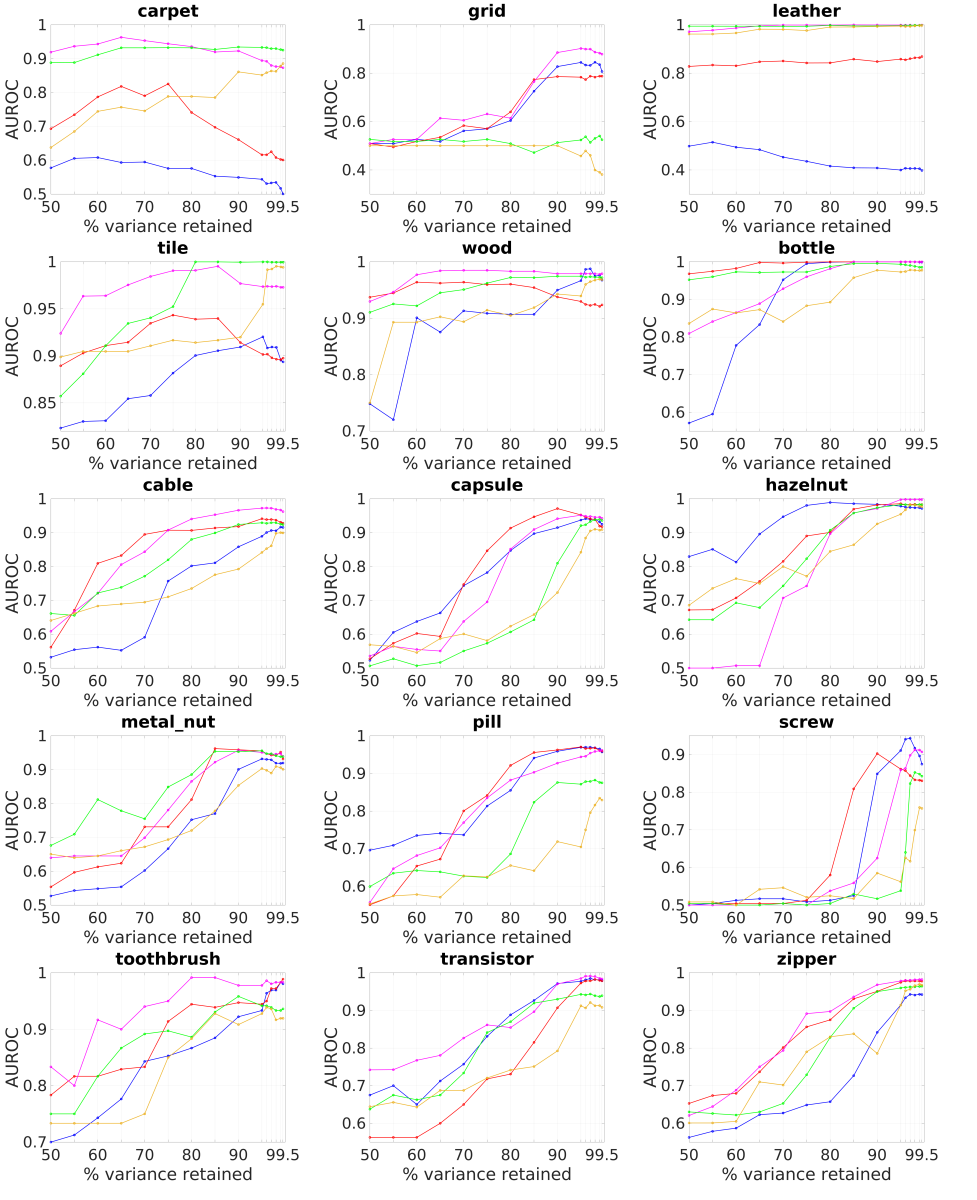


Figure 4: Class-itemized detection results (AUROC) while varying the only parameter of our method used with a ResNet50 backbone. Blue, red, magenta, green and gold resp. denote the following layers: layer1, layer2, layer3, layer4, and avgpool. They show insensitivity to parametrization, esp. within reasonable bounds $[0.95, 1.0)$

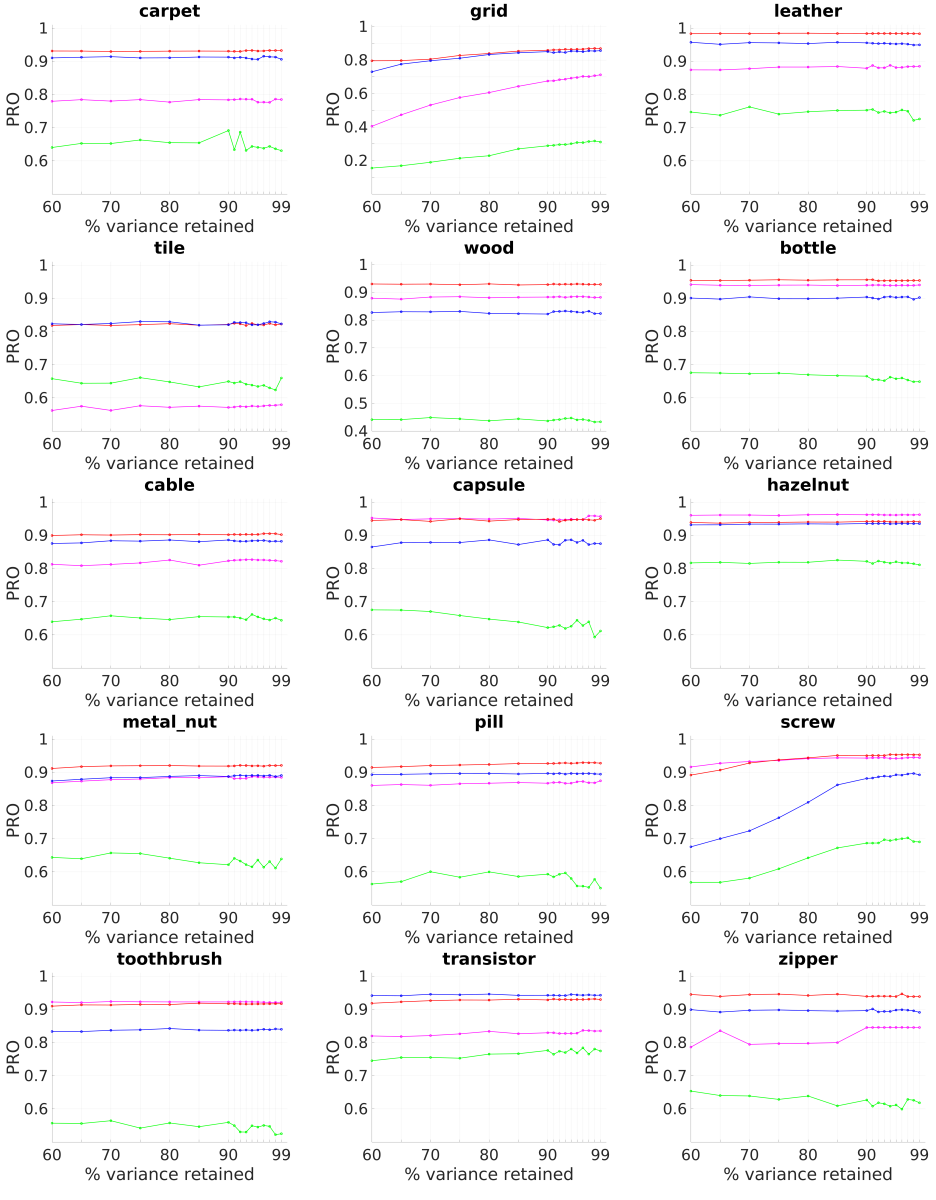


Figure 5: Class-itemized segmentation results (PRO) while varying the only parameter of our method used with a ResNet50 backbone. Blue, red, magenta, and green resp. denote the following layers: layer1, layer2, layer3, and layer4. They show insensitivity to parametrization, esp. within reasonable bounds $[0.95, 1.0)$

| | CNN (Dict)[8] | AE (L2)[8] | SPADE[8] | PaDiM[8] | PatchCore[8] | AST[8] | FRE (1L & 3L) | |
|---|---|---|---|---|---|---|---|---|
| Carpet | 72 | 59 | 97.5 | 99.1 | 99 | - | 98.3 | 99.2 |
| Grid | 59 | 90 | 93.7 | 97.3 | 98.7 | - | 97.3 | 98.1 |
| Leather | 87 | 75 | 97.6 | 99.2 | 99.3 | - | 99.8 | 99.8 |
| Tile | 93 | 51 | 87.4 | 94.1 | 95.6 | - | 95.1 | 96.5 |
| Wood | 91 | 73 | 88.5 | 94.9 | 95 | - | 96.7 | 97.7 |
| Bottle | 78 | 86 | 98.4 | 98.3 | 98.6 | - | 98.7 | 98.8 |
| Cable | 79 | 86 | 97.2 | 96.7 | 98.4 | - | 97.4 | 97 |
| Capsule | 84 | 88 | 99 | 98.5 | 98.8 | - | 98.8 | 99.1 |
| Hazelnut | 72 | 95 | 99.1 | 98.2 | 98.7 | - | 98.7 | 99.1 |
| Metal nut | 82 | 86 | 98.1 | 97.2 | 98.4 | - | 96.6 | 97.3 |
| Pill | 68 | 85 | 96.5 | 95.7 | 97.4 | - | 96.9 | 97 |
| Screw | 87 | 96 | 98.9 | 98.5 | 99.4 | - | 98.9 | 99.2 |
| Toothbrush | 77 | 93 | 97.9 | 98.8 | 98.7 | - | 98.4 | 98.7 |
| Transistor | 66 | 86 | 94.1 | 98.5 | 96.3 | - | 96.3 | 96.5 |
| Zipper | 76 | 77 | 96.5 | 98.5 | 98.8 | - | 98.6 | 98.8 |
| **Average** | **78** | **82** | **96** | **97.5** | **98.1** | **95.0** | **97.8** | **98.2** |

Table 6: MVTec Anomaly Segmentation benchmark with pixel-wise AUROC metric.

| | **Efficientnet B5** | | **VGG16** | | **Resnet18** | | **Resnet50** | |
|---|---|---|---|---|---|---|---|---|
| | 1L | 3L | 1L | 3L | 1L | 3L | 1L | 3L |
| carpet | 94.6 | 97.6 | 97.5 | 97.8 | 97.9 | 99.0 | 98.4 | 99.2 |
| grid | 95.0 | 97.3 | 98.2 | 98.5 | 96.7 | 97.4 | 97.3 | 98.1 |
| leather | 98.6 | 99.3 | 98.8 | 99.0 | 99.7 | 99.8 | 99.8 | 99.8 |
| tile | 93.4 | 95.5 | 92.6 | 92.7 | 88.8 | 93.3 | 95.1 | 96.5 |
| wood | 91.7 | 93.8 | 96.2 | 96.3 | 94.6 | 96.6 | 96.7 | 97.7 |
| bottle | 98.6 | 98.3 | 97.9 | 97.6 | 98.4 | 98.6 | 98.7 | 98.8 |
| cable | 96.3 | 96.7 | 95.7 | 95.8 | 95.9 | 96.7 | 97.4 | 97.0 |
| capsule | 98.7 | 98.5 | 99.2 | 99.2 | 98.3 | 98.9 | 98.8 | 99.1 |
| hazelnut | 98.3 | 98.1 | 98.8 | 98.9 | 98.3 | 99.0 | 98.8 | 99.1 |
| metal nut | 96.2 | 95.5 | 96.3 | 96.4 | 95.4 | 97.0 | 96.6 | 97.3 |
| pill | 96.4 | 96.1 | 97.5 | 97.6 | 96.1 | 97.0 | 96.9 | 97.0 |
| screw | 98.4 | 98.1 | 99.5 | 99.6 | 99.1 | 99.3 | 98.9 | 99.2 |
| toothbrush | 98.3 | 97.9 | 98.5 | 98.5 | 98.2 | 98.9 | 98.4 | 98.7 |
| transistor | 95.4 | 96.7 | 95.6 | 95.6 | 95.6 | 96.4 | 96.3 | 96.5 |
| zipper | 96.9 | 97.7 | 98.3 | 98.0 | 98.4 | 98.8 | 98.6 | 98.8 |
| **Average** | **96.4** | **97.2** | **97.4** | **97.4** | **96.8** | **97.8** | **97.8** | **98.2** |

Table 7: MVTec Anomaly Segmentation: pixel-wise AUROC for FRE across backbones

| | Layer1 | Layer2 | Layer3 | Layer4 |
|---|---|---|---|---|
| carpet | 78.48 | 93.07 | 94.21 | 78.10 |
| grid | 71.36 | 87.21 | 89.29 | 48.97 |
| leather | 88.10 | 98.31 | 97.56 | 79.24 |
| tile | 57.87 | 82.49 | 82.71 | 70.89 |
| wood | 88.25 | 92.66 | 89.58 | 53.39 |
| bottle | 94.09 | 95.45 | 93.22 | 76.90 |
| cable | 82.02 | 90.21 | 85.04 | 70.86 |
| capsule | 95.90 | 94.34 | 91.75 | 68.69 |
| hazelnut | 96.25 | 94.06 | 93.10 | 84.86 |
| metal nut | 88.46 | 92.00 | 91.49 | 74.40 |
| pill | 87.34 | 93.01 | 90.41 | 72.29 |
| screw | 94.39 | 95.44 | 93.88 | 74.63 |
| toothbrush | 92.13 | 91.58 | 89.93 | 59.14 |
| transistor | 83.14 | 92.86 | 94.72 | 84.62 |
| zipper | 84.53 | 94.63 | 93.07 | 71.96 |
| Average | **85.49** | **92.49** | **91.33** | **71.26** |

Table 8: PRO across Resnet50 layers

| | Layer1 | Layer2 | Layer3 | Layer4 |
|---|---|---|---|---|
| carpet | 92.01 | 98.35 | 98.68 | 96.11 |
| grid | 90.66 | 97.28 | 97.57 | 81.92 |
| leather | 96.12 | 99.76 | 99.49 | 98.11 |
| tile | 83.15 | 95.09 | 95.22 | 94.17 |
| wood | 94.57 | 96.67 | 95.75 | 86.28 |
| bottle | 97.93 | 98.71 | 98.27 | 95.71 |
| cable | 94.72 | 97.37 | 95.56 | 93.11 |
| capsule | 98.62 | 98.81 | 98.37 | 95.62 |
| hazelnut | 98.87 | 98.75 | 98.35 | 96.83 |
| metal nut | 95.82 | 96.63 | 96.66 | 92.18 |
| pill | 94.24 | 96.86 | 95.64 | 93.57 |
| screw | 98.46 | 98.94 | 98.27 | 94.79 |
| toothbrush | 98.05 | 98.37 | 98.22 | 92.66 |
| transistor | 92.30 | 96.30 | 96.54 | 91.44 |
| zipper | 94.89 | 98.61 | 98.63 | 95.51 |
| Average | **94.69** | **97.77** | **97.41** | **93.2** |

Table 9: pixel-wise AUROC across Resnet50 layers

# References

[1] Paul Bergmann, Michael Fauser, David Sattlegger, and Carsten Steger. Mvtec ad–a comprehensive real-world dataset for unsupervised anomaly detection. In *Proceedings of the IEEE/CVF Conference on Computer Vision and Pattern Recognition*, pages 9592–9600, 2019.

[2] Niv Cohen and Yedid Hoshen. Sub-image anomaly detection with deep pyramid correspondences. *CoRR*, abs/2005.02357, 2020. URL https://arxiv.org/abs/2005.02357.

[3] Thomas Defard, Aleksandr Setkov, Angelique Loesch, and Romaric Audigier. Padim: a patch distribution modeling framework for anomaly detection and localization. *CoRR*, abs/2011.08785, 2020. URL https://arxiv.org/abs/2011.08785.

[4] P. Napoletano, F. Piccoli, and R. Schettini. Anomaly detection in nanofibrous materials by cnn-based self-similarity. *Sensors*, 18, 2018.

[5] K. Roth, L. Pemula, J. Zepeda, B. Schölkopf, T. Brox, and P. V. Gehler. Towards total recall in industrial anomaly detection. *CoRR*, abs/2106.08265, 2021.

[6] Marco Rudolph, Tom Wehrbein, Bodo Rosenhahn, and Bastian Wandt. Asymmetric student-teacher networks for industrial anomaly detection. In *Winter Conference on Applications of Computer Vision (WACV)*, January 2023.